The Role of Model Weighting Functions in the Gravity and DC Resistivity Inversion

Ramin Varfinezhad, Maurizio Fedi, and Maurizio Milano

***Abstract*— This article aims at analyzing the inversion with the mostly used model weighting functions for both gravity and dc resistivity data. We show that the model weighting function built with depth weighting and compacting factor, formerly formulated for the gravity and magnetics problems, can be useful also for dc resistivity data. We provide a number of synthetic cases to discuss the pros and cons of each model-weighting function. For gravity and dc resistivity data, the comparison was made using the depth weighting with different exponents, the compactness, and, for the dc resistivity nonlinear problem, the roughness matrix under the L_1- and L_2-norm constrained optimizations. As for the depth weighting, the value of the β exponent is decisive for the gravity problem, ranging from very low values for interfaces to 1 for compact sources. The dc resistivity data inversion is less sensitive to β, but the above-indicated choice leads to faster convergence. Similarly, the role of compactness is decisive for reconstructing a compact source from gravity, while, for dc resistivity, it is especially useful to warrant an even faster convergence. Using the roughness matrix tends instead to provide a decrease in resolution at depth. We obtained interesting results for different types of dc resistivity arrays: the weighting function built with depth-weighting and compactness yields a more coherent source reconstruction than that using the roughness matrix. We also analyze two different real dc resistivity cases, which confirms, again, the usefulness of the depth weighting and compactness to model the deep resistive sources.**

***Index Terms*— Compactness, dc resistivity, depth weighting, gravity, inversion, model weighting.**

I. Introduction

GRAVITY and magnetic forward problems are linear problems versus density and susceptibility, respectively, and have the form of the Fredholm integral equation of the first kind. The dc resistivity problem is nonlinear versus resistivity, but it may be linearized under the Born approximation [1], so assuming again the form of a Fredholm integral equation of the first kind.

For these problems, the ambiguity of the related model can only be overcome by providing prior information on the source model. This is usually done by bounding the source-property values or using local constraints from external information (well logs, rock samples, and other geophysics models). However, the fundamental nonuniqueness of the inverse problems may also be reduced by supplying *a priori* information through a model-weighting function, whose role is the object of this article.

To solve a linear problem $\mathbf{d} = \mathbf{Am}$, where $\mathbf{d}$ and $\mathbf{m}$ are the data and model vectors and $\mathbf{A}$ is the kernel matrix, the typical approach is considering the problem as mixed-determined and searching for a solution that minimizes some combination of the data prediction error $\mathbf{d}^{\mathrm{T}}\mathbf{d}$ and the solution length, $\mathbf{m}^{\mathrm{T}}\mathbf{m}$. This last choice means that we are searching for the smallest (or simplest) solution. However, either $\mathbf{d}^{\mathrm{T}}\mathbf{d}$ or $\mathbf{m}^{\mathrm{T}}\mathbf{m}$ are not very good measures of the prediction error and the solution's simplicity. The prediction error is so modified in $\mathbf{d}^{\mathrm{T}}\mathbf{W}_d\mathbf{d}$, where the matrix $\mathbf{W}_d$ defines the relative contribution of each individual error to the total prediction error. Regarding the solution length, it is well known to potential fields practitioners that the smallest solution requirement, a minimum of $\|\mathbf{m}^{\mathrm{T}}\mathbf{m}\|_2$, leads to the shallowest possible solution, which is often a not sound solution, from the geophysical point of view. Thus, a model weighting matrix $\mathbf{W}_m$ is introduced so that the solution simplicity, generalized as $\mathbf{m}^{\mathrm{T}}\mathbf{W}_m\mathbf{m}$, could allow the source models to meet different requirements. For instance, we may request the source to be relatively flat or smooth by using the flatness or roughness matrix $\mathbf{D}$, or we may require the source to be compact. Furthermore, we may desire that the source could be approximately at some depth (see [2] and [3]).

During the last decades, many algorithms have been introduced for dc resistivity (e.g., [1] and [4]–[14]) and gravity data inversions (e.g., [2], [3], and [16]–[21]).

In this article, we will analyze the different responses given by dc resistivity and gravity data under various choices for the weighting matrix $\mathbf{W}_m$. To this end, we will use the weighted damped least-squares algorithm [22] with the linearized integral form of the dc resistivity problem (see [6] and [23]) and the gravity integral equation. For the dc resistivity problem, we will also use the L_2- and L_1-norm constrained optimization methods [24].

II. Methodology

A. DC Resistivity and Gravity Forward Problems

Considering a half-space υ with conductivity $\sigma(\mathbf{r})$, the potential $\varphi(\mathbf{r}_{\mathrm{obs}})$ at the surface due to a point source of intensity I can be expressed as (e.g., [25])

$$\varphi(\mathbf{r}_{\mathrm{obs}}) = \frac{I}{2\pi\,|\mathbf{r}_S - \mathbf{r}_{\mathrm{obs}}|\sigma_s} + \frac{1}{2\pi}\int_{\upsilon}\frac{\nabla\sigma(\mathbf{r})}{\sigma(\mathbf{r})}\cdot\frac{\nabla\varphi(\mathbf{r})}{|\mathbf{r}-\mathbf{r}_{\mathrm{obs}}|}\mathrm{d}\upsilon \qquad (1)$$

Manuscript received September 15, 2021; revised December 8, 2021; accepted December 29, 2021. Date of publication February 4, 2022; date of current version March 23, 2022. *(Corresponding author: Ramin Varfinezhad.)*

Ramin Varfinezhad is with the Department of Physics of Earth, Institute of Geophysics, University of Tehran, Tehran 5115414399, Iran (e-mail: ramin.varfi@ut.ac.ir).

Maurizio Fedi is with the Department of Earth, Environment and Resources Sciences, University of Naples Federico II, 80138 Naples, Italy.

Maurizio Milano is with the Institute of Marine Sciences of Naples—National Research Council (ISMAR CNR), 80133 Naples, Italy.

Digital Object Identifier 10.1109/TGRS.2022.3149139

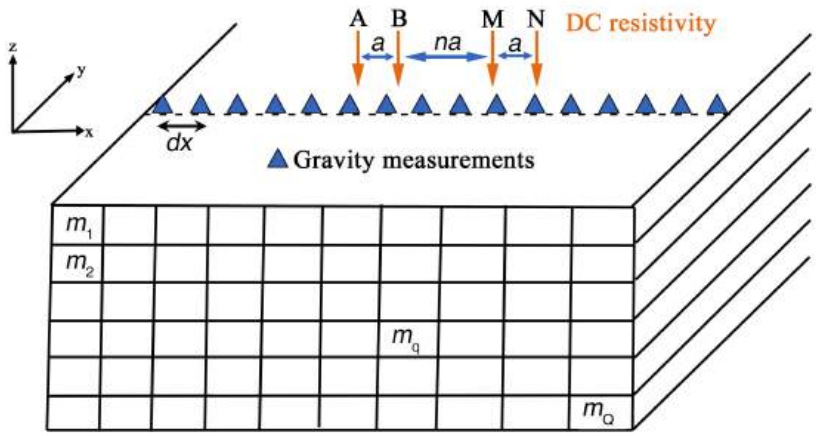

Fig. 1. Discretization of the source volume into a set of prisms with constant resistivity and density. A dipole–dipole array is considered for dc resistivity.

where $\mathbf{r}_S$ and $\mathbf{r}_{\text{obs}}$ are the source and the observation position vectors, respectively.

Equation (1) indicates that the potential forward problem relative to the dc resistivity method is nonlinear. However, Perez-Flores *et al.* [1], assuming dc resistivity measurements with four electrode arrays, used the Born approximation to write apparent resistivity ($\log\rho_a$) as a linear function of the true resistivity $\log\rho$

$$\log\rho_a(\mathbf{r}_A,\mathbf{r}_B,\mathbf{r}_M,\mathbf{r}_N) = \frac{[h]^{-1}}{\pi}\int_{v'} K(\mathbf{r}_A,\mathbf{r}_B,\mathbf{r}_M,\mathbf{r}_N,\mathbf{r}')\log\rho(\mathbf{r}')d^3r' \tag{2}$$

where

$$K(\mathbf{r}_A,\mathbf{r}_B,\mathbf{r}_M,\mathbf{r}_N,\mathbf{r}') = N(\mathbf{r}_A,\mathbf{r}_M,\mathbf{r}') - N(\mathbf{r}_B,\mathbf{r}_M,\mathbf{r}') - N(\mathbf{r}_A,\mathbf{r}_N,\mathbf{r}') + N(\mathbf{r}_B,\mathbf{r}_N,\mathbf{r}') \tag{3}$$

with

$$N(\mathbf{r}_i,\mathbf{r}_j,\mathbf{r}') = \frac{(\mathbf{r}'-\mathbf{r}_i)\cdot(\mathbf{r}_j-\mathbf{r}')}{|\mathbf{r}'-\mathbf{r}_i|^3|\mathbf{r}_j-\mathbf{r}'|^3} \tag{4}$$

and h is the geometrical factor, which is related to the array type.

In the 2-D case, we assume that the resistivity does not change along the y-direction, and the array is along the x-axis, with coordinates x_A, x_B, x_M, and x_N of electrodes A, B, M, and N, respectively. Putting $y=0$ and $z=0$ (i.e., flat topography), the integral equation simplifies to:

$$\log\rho_a(x_A,x_B,x_M,x_N) = \frac{[h]^{-1}}{\pi} \times \int_{\Delta x}\int_{\Delta z} K(x_A,x_B,x_M,x_N,x',z') \times \log\rho(x',z')dx'dz' \tag{5}$$

where the vertical section is sized $\Delta x \times \Delta z$ and

$$K(x_A,x_B,x_M,x_N,x',z') = N(x_A,x_M,x',z') - N(x_B,x_M,x',z') - N(x_A,x_N,x',z') + N(x_B,x_N,x',z') \tag{6}$$

with [26]

$$N(x_i,x_j,x',z') = \int_{-\infty}^{\infty} \frac{(x'-x_i)(x_j-x') - y'^2 - z'^2}{\sqrt{\left((x'-x_i)^2+y'^2+z'^2\right)^3\left((x_j-x')^2+y'^2+z'^2\right)^3}}dy' \quad \begin{cases} i = A, B \\ j = M, N. \end{cases} \tag{7}$$

If we have P measured data and discretize the source volume of vertical section $\Delta x \times \Delta z$ into Q prismatic cells of infinite length in the y-direction and constant resistivity (see Fig. 1), we form the system

$$\mathbf{d} = \mathbf{A}\mathbf{m} \tag{8}$$

where $\mathbf{d}$ is the data vector, containing the $\log(\rho_a)$ data, $\mathbf{m}$ is the model vector, containing the $\log(\rho)$ unknowns, and $\mathbf{A}$ is a $P \times Q$ matrix, whose elements are given by

$$A_{pq} = \int_{\Delta x_q}\int_{\Delta z_q} K_p(x',z')dx'dz' \tag{9}$$

with $p = 1,\ldots,P$ and $q = 1,\ldots,Q$. Each cell is sized $\Delta x_q \times \Delta z_q$.

Perez-Flores *et al.* [1] computed $\mathbf{A}$ by analytically solving (6). However, we prefer here to compute it numerically because it allows an easier extension to the 2.5-D case. Comparing the response of the linear integral equation with that derived from standard software (Res2dmod [27]), we found differences of less than 5% in the logarithm of resistivities, even considering rather rough meshes for the subsurface.

We considered three numerical techniques to solve the linear integral equation: 1) midpoint rule; 2) trapezoidal rule; and 3) Gauss quadrature technique. By the first one, the integral value is approximated in each interval by a formula based on its midpoint, while the last two methods use formulas based on two points. Therefore, the midpoint rule leads to the fastest estimation of the integral, while trapezoidal and Gauss quadrature rules are, in general, more precise. However, it should be mentioned that the three algorithms produce similar results when we have a high number of discretization points.

The gravity forward problem is given by the integral equation [3]

$$f(\mathbf{r}) = \gamma \int_V \frac{z - z_0}{|\mathbf{r} - \mathbf{r}_0|^3} \eta(\mathbf{r}_0) d\mathbf{r}_0^3 \tag{10}$$

where γ is the gravitational constant and $\eta(\mathbf{r}_0)$ is the density distribution in the source volume V.

If we have P measured data and discretize the source volume into Q prismatic cells of constant density, we form the system $\mathbf{d} = \mathbf{Am}$, where $\mathbf{d}$ is the gravity data vector and $\mathbf{m}$ is the density model vector. $\mathbf{A}$ is the $P \times Q$ matrix kernel, whose elements A_{pq} expresses the gravity effect at the pth measurement point due to the qth prismatic block

$$A_{pq} = \gamma \int_{V_q} \frac{z_p - z_q}{|\mathbf{r}_p - \mathbf{r}_q|^3} dV \tag{11}$$

with $p = 1, \ldots, P$ and $q = 1, \ldots, Q$. In the 2-D case, we will assume that the blocks have an infinite length along the y-direction.

B. Gravity and DC Resistivity Inverse Problems

Since both the problems are under the form of a Fredholm integral equation of the first kind, we solve both the inverse problems by minimizing the objective function

$$\|\mathbf{W}_d(\mathbf{Am} - \mathbf{d})\|_2^2 + \mu \|\mathbf{W}_m(\mathbf{m} - \mathbf{m_0})\|_2^2 \tag{12}$$

where $\mathbf{m}_0$ is the starting model, μ is the regularizing factor, and $\mathbf{W}_d$ and $\mathbf{W}_m$ are the data and model weighting functions, respectively. In all cases, $\mathbf{m}_0$ is zero for gravity, while it is a homogenous model for dc resistivity, with the resistivity equal to the mean of the apparent resistivities. For simplicity, we will here assume independent measurements with unit variance so that $\mathbf{W}_d = \mathbf{I}$. As for the appropriate choice of μ, we used the generalized cross-validation (GCV) technique (e.g. [28]). For the dc resistivity problem, we will use the approximate integral linear equation of the true nonlinear problem [from now on, LE; see (8)] or an optimization method solving the nonlinear dc resistivity problem, based on (1) (from now on, NLE). To this end, we will use the "weighted damped least-squares" algorithm [22] for solving the LE problem. At each kth step, we may write

$$\mathbf{m}_k = \mathbf{m}_{k-1} + \left(\mathbf{W}_m^{-1}\mathbf{A}^{\mathbf{T}}\right)\left(\mathbf{A}\mathbf{W}_m^{-1}\mathbf{A}^{\mathbf{T}} + \mu\mathbf{W}_d\right)^{-1} \times (\mathbf{d} - \mathbf{Am}_{k-1}). \tag{13}$$

For the NLE resistivity problem, Loke *et al.* [24] described a versatile algorithm, which is implemented in the widespread RES2DINV[1] software. It refers to two optimization iterative approaches, which may be alternatively selected. The first is the L_2-norm smoothness-constrained optimization method, which produces a model with a smooth variation of resistivity. By this algorithm we minimize, at each kth iteration, the objective function is

$$\Psi(\mathbf{m}_k) = \mathbf{g}_k^{\mathrm{T}}\mathbf{g}_k + \mu_k \mathbf{m}_k^{\mathrm{T}}\mathbf{W}_m\mathbf{m}_k. \tag{14}$$

At the kth iteration, μ_k is the regularization parameter, $\mathbf{m}_k$ is the model vector, and $\mathbf{g}_k = \mathbf{d} - F(\mathbf{m}_k)$ is the data-misfit vector between the logarithm of the apparent resistivity obtained from measurements and that calculated from the model $\mathbf{m}_k$. Based on the gradient of the objective function, the Gauss–Newton method of least squares is used to solve the following system of equations (e.g., [7]):

$$\left(\mathbf{J}_k^{\mathrm{T}}\mathbf{J}_k + \mu_k\mathbf{W}_m\right)\mathbf{\Delta m}_k = \mathbf{J}_k^{\mathrm{T}}\mathbf{g}_k - \mu_k\mathbf{W}_m\mathbf{m}_{k-1} \tag{15}$$

where $\mathbf{J}_k$ is the Jacobian matrix. Once the model variation $\mathbf{\Delta m}_k$ is estimated, the model is updated as $\mathbf{m}_k = \mathbf{m}_{k-1} + \Delta\mathbf{m}_k$.

The second method is an L_1-norm-based optimization method based on the iteratively reweighted least-squares algorithm [29]

$$\left(\mathbf{J}_k^{\mathrm{T}}\mathbf{J}_k + \mu_k\mathbf{W}_m\right)\mathbf{\Delta m}_k = \mathbf{J}_k^{\mathrm{T}}\mathbf{R}_d\mathbf{g}_k - \mu_k\mathbf{W}_m\mathbf{m}_{k-1} \tag{16}$$

where $\mathbf{R}_d$ is a reweighting matrix.

For the gravity problem, data are linearly related to density [see (10)], and we will use the weighted damped least-squares algorithm [see (13)].

C. Model Weighting Function

Based on the above equations, we will consider in this article four types of $\mathbf{W}_m$.

1) *Depth Weighting:* $\mathbf{W}_m = (1/z^\beta)\mathbf{I}$ [relative to the integral equation in (12)], where $0 < \beta < 1$ and z refers to the depths to the center of the blocks: $[z_1, \ldots, z_q, \ldots, z_Q]$. For more details on the depth weighting, see [3] and [17].
2) *Depth Weighting and Compactness [Relative to the Integral Equation in (12)]:* In this case, the weighting function $\mathbf{W}_m$ is updated at each iteration k as $\mathbf{W}_{m_k} = (1/(\mathbf{m}_{k-1} + \varepsilon)^2)(1/z^\beta)\mathbf{I}$, making the relationship between model and data in (13) nonlinear. The compactness constraint, $(\mathbf{m}_{k-1} + \varepsilon)^{-2}$, introduced by Last and Kubic [16], minimizes at each kth iteration the area of the anomalous body in the 2-D section; ε is a very small quantity.
3) *Roughness Matrix [in (15)] for the L_2-Norm Nonlinear Optimization Method:* $\mathbf{W}_m = \alpha_x\mathbf{C}_x^{\mathrm{T}}\mathbf{C}_x + \alpha_z\mathbf{C}_z^{\mathrm{T}}\mathbf{C}_z$, where $\mathbf{C}_x$ and $\mathbf{C}_z$ are the roughness matrices (such as the first-order difference matrix) in the x- and z-directions, respectively, and α_x and α_z are the relative coefficients.
4) *Roughness Matrix [in (16)] for the L_1-Norm Nonlinear Optimization Method:* $\mathbf{W}_m = \alpha_x\mathbf{C}_x^{\mathrm{T}}\mathbf{R}_m\mathbf{C}_x + \alpha_z\mathbf{C}_z^{\mathrm{T}}\mathbf{R}_m\mathbf{C}_z$, where $\mathbf{C}_x$ and $\mathbf{C}_z$ are the roughness matrices (such as the first-order difference matrix) in the x- and z-directions,

[1]Registered trademark.

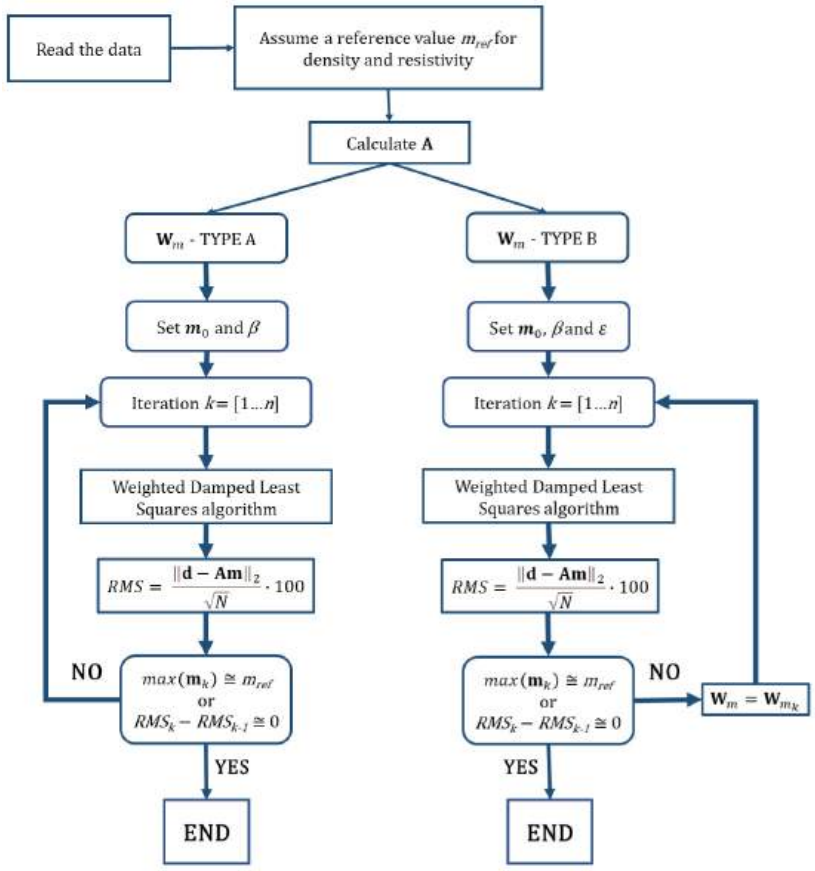

Fig. 2. Flowchart of the LE inversion algorithm for model weighting functions of types A and B.

respectively; α_x and α_z are the relative coefficients, and $\mathbf{R}_d$ and $\mathbf{R}_m$ are reweighting matrices.

Fig. 2 shows the flowchart of the LE inversion algorithm [see (13)], for the model weighting functions in 1) and 2).

For cases 3) and 4), we will use the nonlinear optimization algorithm implemented in the Res2Dinv software [24].

III. Synthetic Modeling

We here consider different synthetic models. The first of them is a dense/resistive block within a less dense/conductive homogenous background. The second case is an interface model, while the third case regards a small conductive body and a faulted resistive block; finally, we consider also a group of conductive bodies of different shapes and depths in a homogeneous half-space. Res2Dmod software is used for calculating the resistivity model forward responses.

The rms error percentage is computed for each obtained solution according to

$$\text{rms} = \frac{\|\mathbf{d} - \mathbf{d}_{\text{cal}}\|_2}{\sqrt{N}} 100 \tag{17}$$

where N is the number of data, $\mathbf{d}$ is the measured data, and $\mathbf{d}_{\text{cal}}$ is the calculated data from the current estimated model $\mathbf{m}_{\text{k}}$. A unit-standard deviation is inherently assumed.

Regarding the inversion of the gravity data, the role of depth weighting and compactness is relatively well known in the relative literature (see [1], [2], [16], and [30]). However, we here introduce the appropriate depth weighting exponent for an interface-like source, which, to the best of our knowledge, has not been discussed in the current literature. In any case, our main interest in this article is comparing the effect of the model weighting function for sources of similar shape in the inversion of both gravity and resistivity data.

A. Resistive/Dense Block Model

The first synthetic case is a dense block model having a 2000-kg/m^3 density contrast [see Fig. 3(a)]. The same body has 100-Ωm resistivity in a homogenous background with a resistivity of 10 Ωm [see Fig. 3(b)]. In both cases, we have 100 data and 500 unknowns. Gaussian random noise of 5% of the data magnitude was added to the data. For the apparent resistivities, the dipole separation (a) is 20, and n is from 1 to 5. The reconstructed models are displayed in Figs. 4 (gravity) and 5 (resistivity), respectively, with weighting functions of types A and B. For each case, the iterative process is stopped automatically when the maximum of $\mathbf{m}_k$ is almost equal to a reference value of ρ (or η) that is assumed a

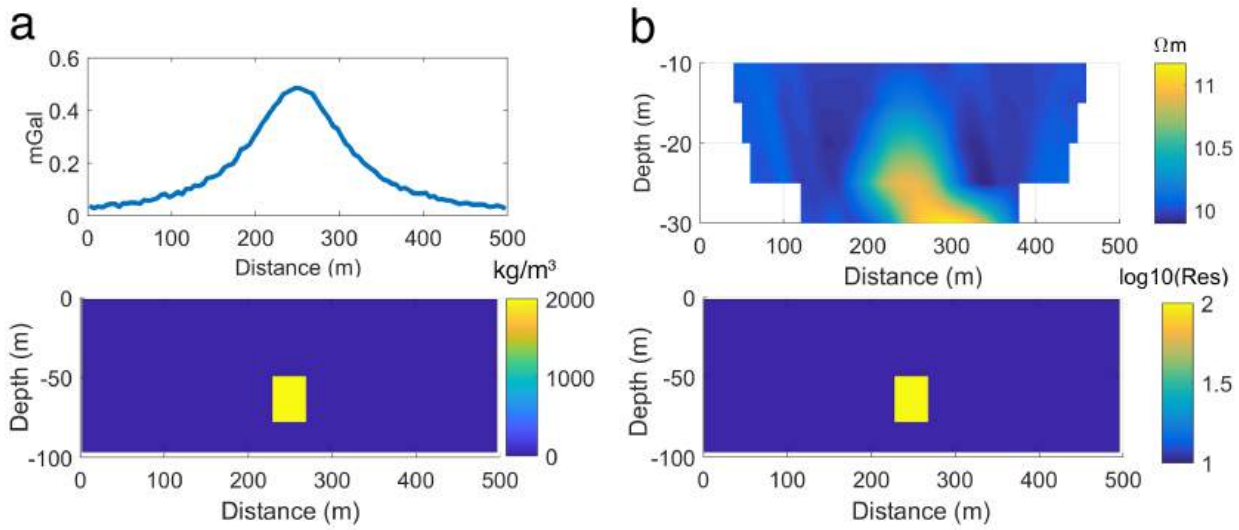

Fig. 3. (a) Gravity anomaly profile and (b) apparent resistivity of a dense/resistive prismatic source.

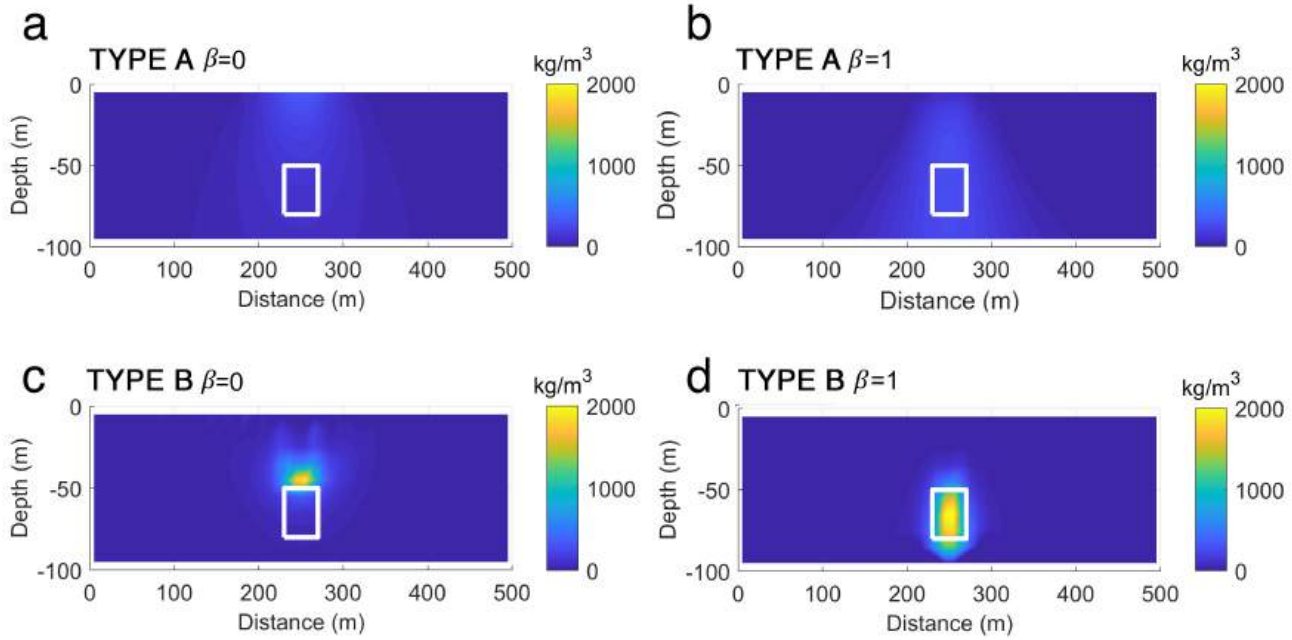

Fig. 4. Density model using the weighting function of type A: (a) with $\beta = 0$ and (b) with $\beta = 1$. The density model using the weighting function of type B: (c) with $\beta = 0$ and (d) $\beta = 1$.

priori (m_{ref} in Fig. 2), or when the rms value does not change significantly.

Our results show that the following holds.

1) For the weighting function of type A and $\beta = 0$, the inversion of the gravity data yields a very shallow density distribution with a low-density contrast [see Fig. 4(a)]; using $\beta = 1$, the source is found to be deeper, well centered to the source depth, but too smooth and with again a low-density contrast [see Fig. 4(b)]. On the other hand, by implementing also compactness besides depth weighting (weighting function of type B), the results are largely improved for both $\beta = 0$ or $\beta = 1$ [see Fig. 4(c) and (d)]. $\beta = 1$, however, provides the best result in terms of depth to the source and density contrast. We also note that the number of iterations required to reasonably fit the data is much smaller for $\beta = 1$ (see Table I). Thus, compactness is particularly useful to largely reduce the computational cost.
2) As for the resistivity data inversion, the use of weighting functions of types A and B gives similar results for $\beta = 0$ and $\beta = 1$ [see Fig. 5(a) and (d)]. However, the number of iterations required to infer the right depth to the source and an acceptable resistivity value is dramatically high if we use the wrong beta exponent ($\beta = 0$) compared to using $\beta = 1$ (see Table I). As for the gravity case, the use of compactness (weighting function

TABLE I

NUMBER OF ITERATIONS AND rms ERROR FOR GRAVITY AND RESISTIVITY DATA INVERSION OF A BLOCK-MODEL USING MODEL WEIGHTING FUNCTION OF TYPES A–C

SINGLE BLOCK MODEL												
$\mathbf{W}_m$	TYPE A $\beta=0$		TYPE A $\beta=1$		TYPE B $\beta=0$		TYPE B $\beta=1$		TYPE C		TYPE D	
	IT	RMS	IT	RMS	IT	RMS	IT	RMS	IT	RMS	IT	RMS
Gravity	5000	2.38	500	1.72	100	3.09	10	2.38	-	-	-	-
Resistivity	10000	0.48	1000	0.49	3000	0.57	300	0.49	5	2.58	5	2.50

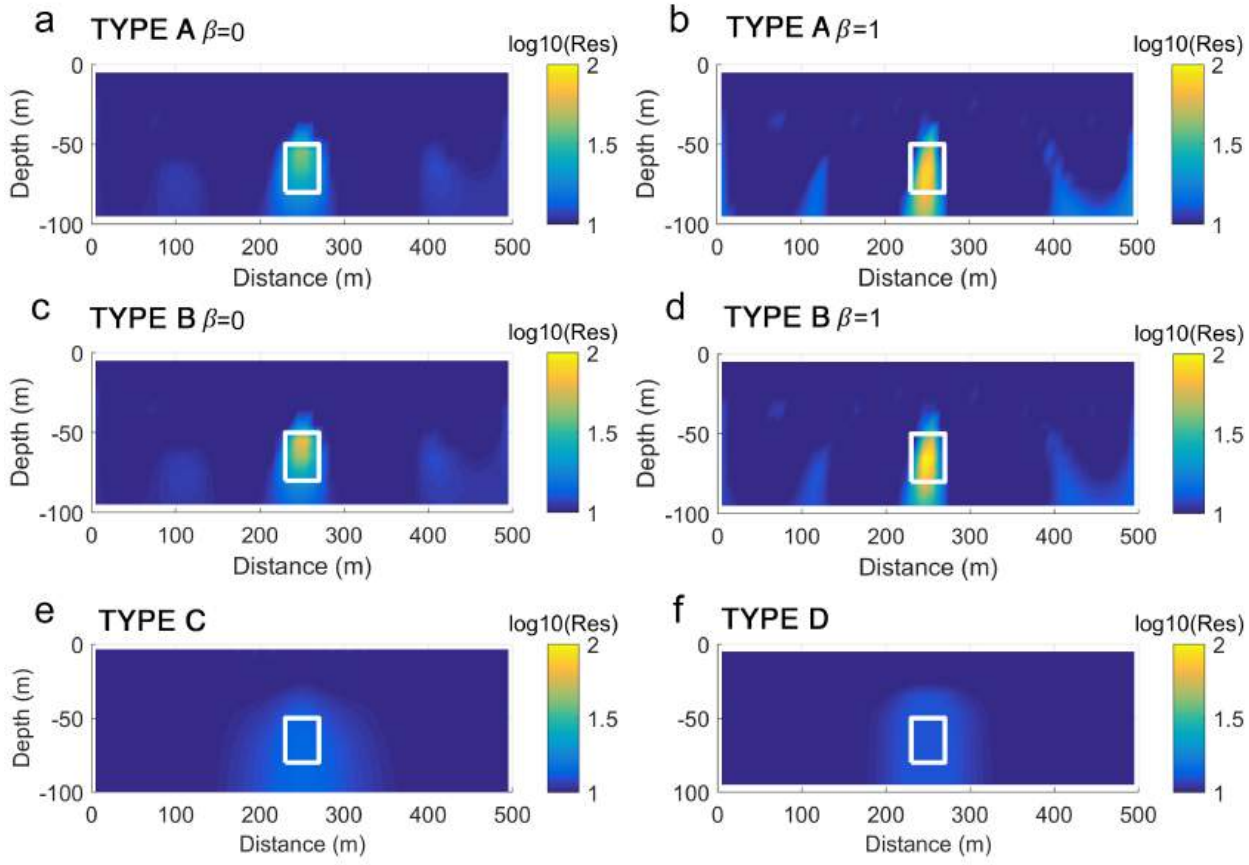

Fig. 5. Resistivity model for the prismatic block using different weighting functions. (a) LE with weighting function of type A and $\beta = 0$. (b) LE with weighting function of type A and $\beta = 1$. (c) LE with weighting function of type B and $\beta = 0$. (d) LE with weighting function of type B and $\beta = 1$. (e) NLE resistivity model using the *L1*-norm. (f) NLE resistivity model using the *L2*-norm.

of type B) reduces consistently the iterative process to more than half of the iterations (see Table I).

3) In Fig. 5(e) and (f), we show the results relative to weighting functions of types C and D. The robust (L_1-norm) model (weighting function of type D) is more well-centered than the least-square (L_2-norm) model (weighting function of type C). However, in both cases, we see that the modeled source is rather deeply and laterally extended with low values of resistivity.

Therefore, the obtained models show that both methods are sensitive to the exponent β of depth weighting; however, gravity inversion has a greater dependence than the dc resistivity inversion since the source position is strongly affected by β. Finally, compactness is significant to reduce the number of iterations and infer the right value of density and resistivity (see Table I).

Consider now a single block close to the surface with a 10-m depth to the top (see Fig. 6). The number of data and dipole

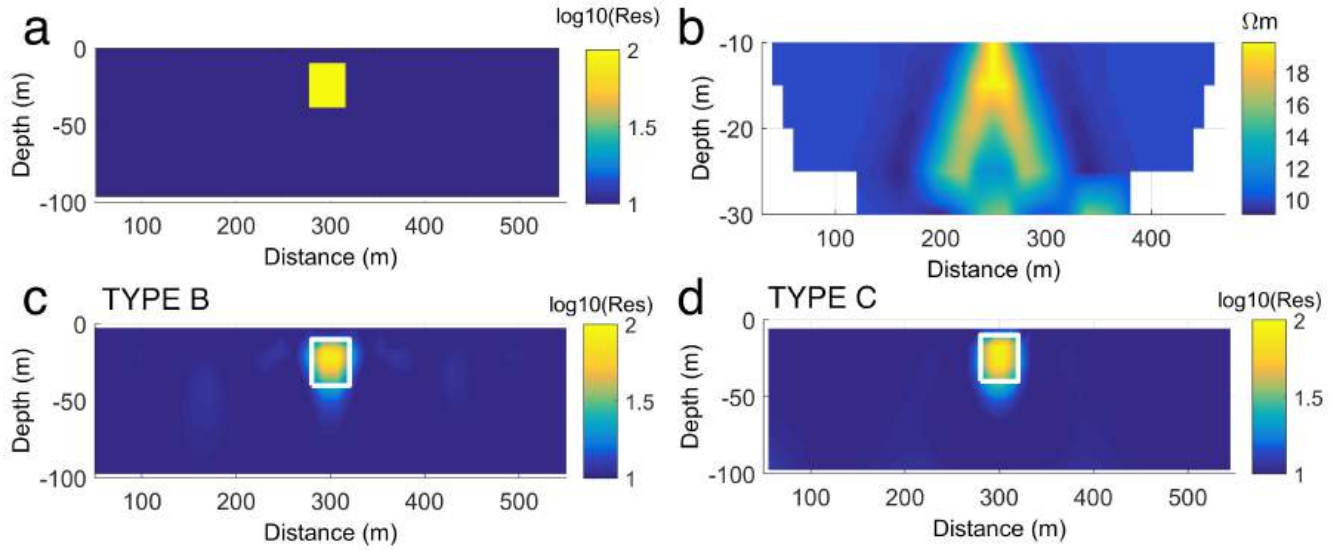

Fig. 6. Resistivity model for (a) shallow block and (b) resistivity pseudosection. Resistivity model obtained using the weighting functions of (c) type B and (d) type C. The source model is much more consistent than that in the case of the deep block (see Fig. 5).

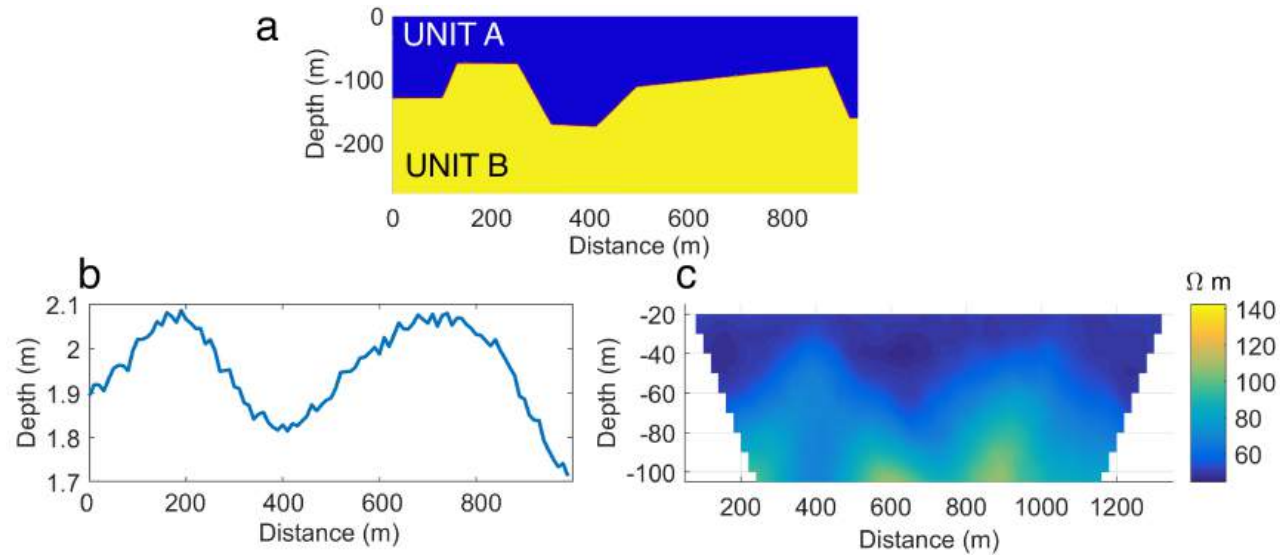

Fig. 7. (a) Interface model consisting of two different units (UNIT A: 50 Ωm–0 kg/m^3; UNIT B: 400 Ωm–300 kg/m^3). (b) Gravity anomaly of the interface model with 5% Gaussian random noise. (c) Apparent resistivity of the interface model with 5% noise.

separation is the same as in the previous case. Resistivity models reconstructed by weighting functions of types B and C demonstrate again their good performance. By comparing this case with that of the deep block, we can clearly notice the important role of depth weighting and compactness in dc resistivity inversion.

We may conclude that the weighting function of type B (depth weighting and compactness) leads to the best result for both gravity and dc resistivity cases, in particular, when the dense/resistive source is not too shallow.

B. Interface Model

We here consider a further synthetic case for dc resistivity and gravity methods, consisting of an interface source model that simulates a real case in the Neapolitan region (Italy). Specifically, the gravity and dc resistivity datasets were generated by modeling the morphology of the interface between the compact Yellow Tuff unit and the overlying loose alluvial materials [31]. The geological interpretations suggested a subsurface geometry consisting of a faulted tuff unit forming two main graben structures [31, Fig. 9].

Our synthetic model is shown in Fig. 7(a) and consists of two homogeneous media with resistivity 50 (Unit A) and 400 Ωm (Unit B). The density contrast between the two homogenous layers is 300 kg/m^3. Dipole separation (a) is 40 m, and n ranges from 1 to 10 for dc resistivity data. A Gaussian random noise of 5% of the data magnitude was added to the data.

We display the gravity anomaly profile and the pseudosection of true resistivity data in Fig. 7(b) and (c), respectively.

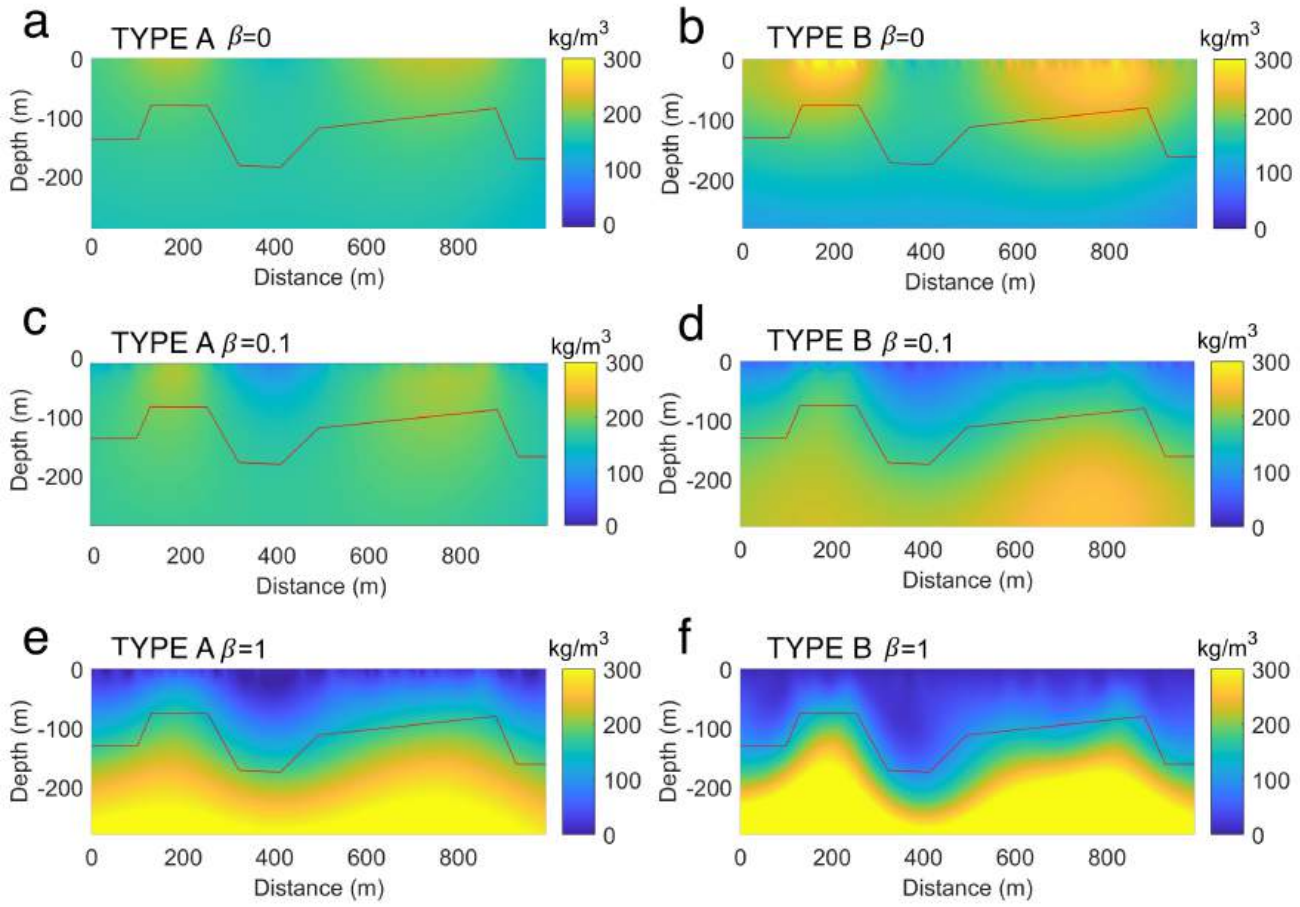

Fig. 8. Interface density model from inversion of gravity data with weighting functions of types A and B. (a) LE with weighting function of type A and β =0. (b) LE with weighting function of type B and β =0. (c) LE with weighting function of type A and β =0.1. (d) LE with weighting function of type B and β =0.1. (e) LE with weighting function of type A and β =1. (f) LE with weighting function of type B and β =1.

Gravity inversion is performed using the weighting functions of type A and type B for three different values of the depth weighting exponent: 0, 0.1, and 1 (see Fig. 8). After the previous case of a homogeneous block, we should expect that the gravity method would be much more sensitive to the depth weighting exponent and compactness than dc resistivity inversion. We see indeed that, even though the data are always well fitted, the resulting models completely differ from each other by setting $\beta = 0$, 0.1, and 1 and, in addition, by making use of compactness.

In fact, it is clear that, with $\beta = 0$ without compactness [see Fig. 8(a)], the inferred model consists of two very shallow sources with low-density values. This is similar to the analogous result for the block source and with the expected result occurring without depth weighting. In fact, $\beta = 0$ means that the weighting function is not active so that a very shallow result is expected by minimizing the objective function. We obtain slightly deeper solutions using $\beta = 0.1$ [see Fig. 8(c)], which are, however, still too shallow with respect to the true source depth. Fig. 8(e), instead, shows that using $\beta = 1$ without compactness the obtained model is, as expected, considerably too deep. On the other hand, compactness with $\beta = 0$ provides a better density estimation, but the sources are too shallow [see Fig. 8(b)]. For $\beta = 1$, the density model is too deep [see Fig. 8(f)]. Finally, with $\beta = 0.1$, we obtain a reconstruction of the interface that is truly consistent with respect to the real model geometry and yields a reasonable density contrast [see Fig. 8(d)]. Note that the optimal choice of the depth weighting exponent for an interface has not yet been discussed in the literature: our result shows that an interface-like source can be modeled from inversion of gravity data, provided that a low value of the depth-weighting exponent is used.

As for the resistivity data, we used weighting functions of types A–D. As for the block model, we may see from Fig. 9 that the depth weighting exponent is not decisive so that the resulting models are equally well reproducing the true source geometry, no matter the choice of β. However, also, in this case, the right choice of β and the compactness are extremely important to reduce considerably the number of iterations required to infer the appropriate values of resistivity. Table II, in fact, shows that, by using $\beta = 0$ without compactness [see Fig. 9(a)], we need up to 1000 iterations to achieve a good interface model. $\beta = 1$ and compactness [see Fig. 9(f)], instead, allow modeling the interface source within just two iterations. As regards the model weighting function of

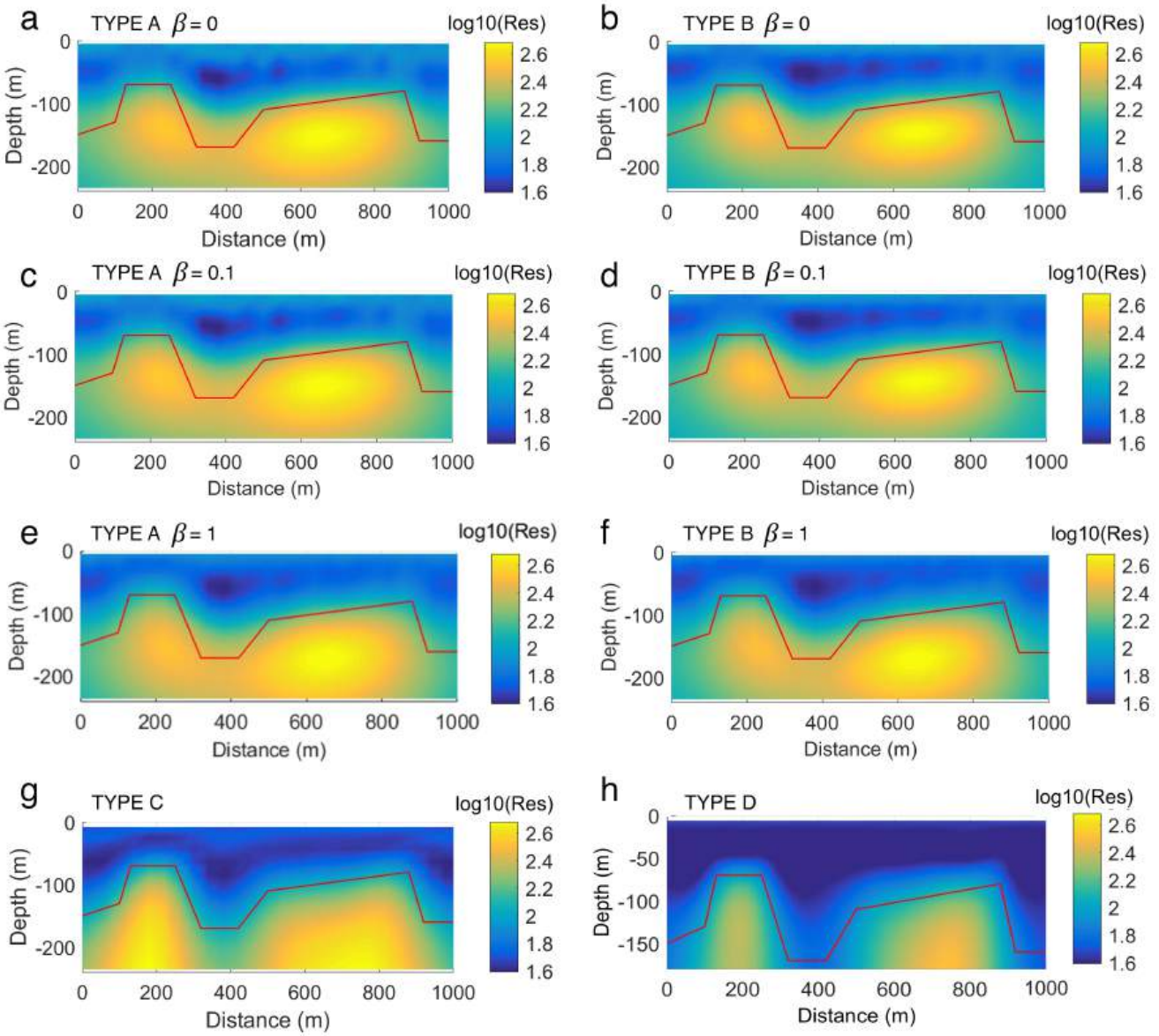

Fig. 9. Resistivity interface models for different types of weighting matrices. (a) and (b) LE for $\beta = 0$ with model weighting functions of types A and B, respectively. (c) and (d) LE for $\beta = 0.1$ with model weighting functions of types A and B, respectively. (e) and (f) LE for $\beta = 1$ with model weighting functions of types A and B, respectively. (g) NLE with a model weighting function of type C. (h) NLE with a model weighting function of type D.

Types C and D (the roughness matrix), the interface is modeled at a quite reasonable depth [see Fig. 9(g)], and few iterations are needed, but the models resemble two distinct bodies rather than an interface.

C. Faulted Block (Contact) and Prismatic Source

As a further synthetic test, we used the default Res2dinv model case of a resistive faulted block and small conductive rectangular prism [32, Fig. 4.5]. Resistivities of the faulted block, background, and small prism are 40, 10, and 1 Ωm, respectively.

We considered two cases for this synthetic case: 1) a faulted block with a shallow compact body and 2) a faulted block with a deep rectangular compact body [see Fig. 10(a) and (b)]. We considered a Wenner–Schlumberger array with 1-m dipole separation. For both cases, we consider n from 1 to 10. We show the inversion results relative to a weighting function of type B and $\beta = 1$ in Fig. 10(e) and (f), while the models obtained by using weighting functions of types C and D are represented in Fig. 10(g)–(j). When the small prismatic body is shallow, we can reproduce both the sources fairly well, no matter the choice of the weighting function.

However, the weighting functions of types B and C [see Fig. 10(e)–(g)] allow a good definition of the faulted block, while we may observe a decreased resolution at depth for the small body. The weighting function of type D provides the best representation of both sources.

On the other hand, when the small block lies at a greater depth [see Fig. 10(b)], we observe significant differences, depending on the choice of the type of weighing function.

TABLE II

NUMBER OF ITERATIONS AND rms ERROR FOR GRAVITY AND RESISTIVITY DATA INVERSION OF THE INTERFACE MODEL USING MODEL WEIGHTING FUNCTIONS OF TYPES A–C

$\mathbf{W}_m$	TYPE A $\beta=0$		TYPE A $\beta=0.1$		TYPE A $\beta=1$	
	IT	RMS	IT	RMS	IT	RMS
Gravity	100	0.1111	50	0.1461	10	0.0021
Resistivity	1000	1.2944	500	1.3395	6	1.2329
$\mathbf{W}_m$	TYPE B $\beta=0$		TYPE B $\beta=0.1$		TYPE B $\beta=0$	TYPE B $\beta=1$
	IT	RMS	IT	RMS	IT	RMS
Gravity	50	0.0126	5	0.0612	2	0.0231
Resistivity	150	1.4249	70	1.5420	2	1.4639

$\mathbf{W}_m$	TYPE C		TYPE D	
	IT	RMS	IT	RMS
Resistivity	5	0.57	5	0.43

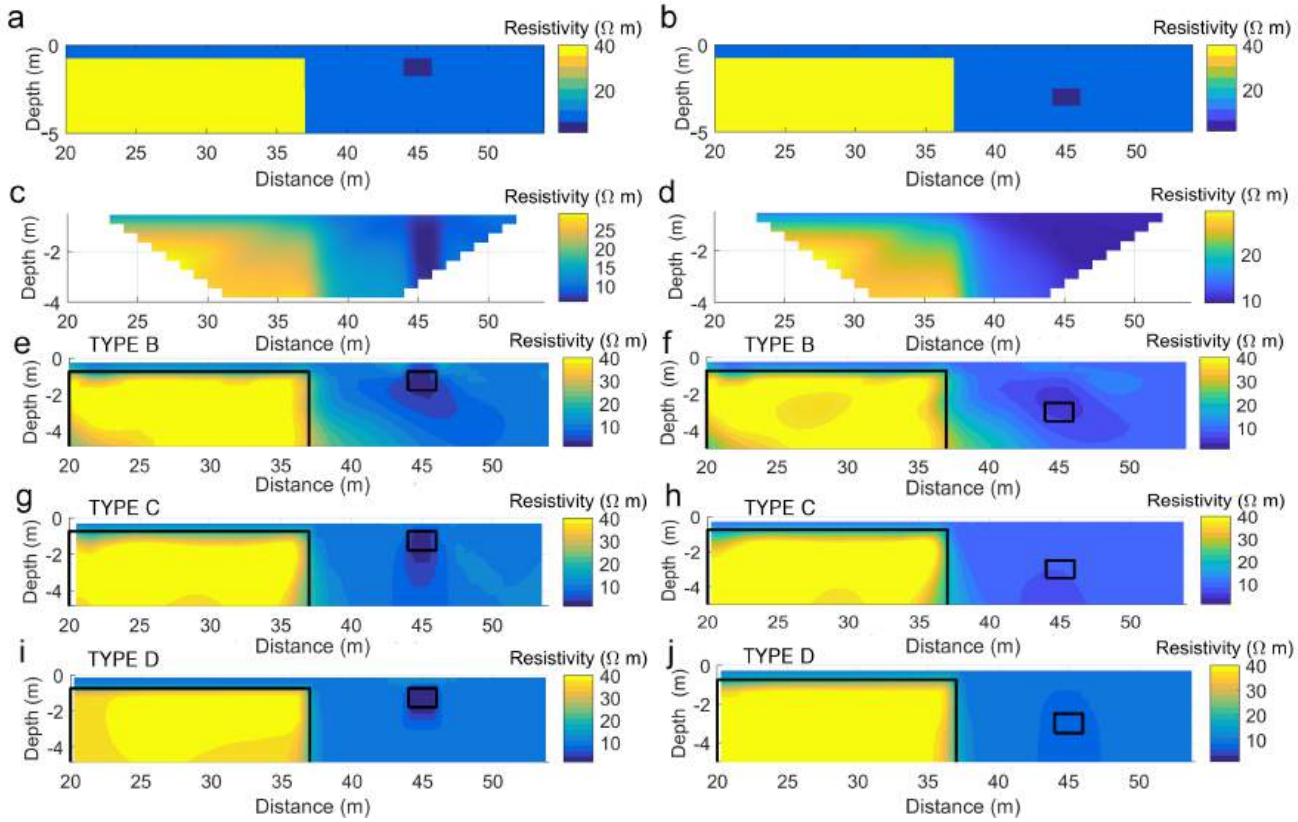

Fig. 10. Resistivity models of a faulted block (contact) with (a) shallow prismatic body and (b) deep prismatic body. (c) and (d) Resistivity pseudosections. (e) and (f) Resistivity models using a weighting function of type B with $\beta = 1$. (g) and (h) Resistivity models using the weighting function of type C. (i) and (j) Resistivity models using a weighting function of type D.

The weighting function of type B, in fact, allows retrieving with enough precision the location and resistivity value of the small prismatic body. Model weighting functions of types C and D, instead, lead to a well-pronounced faulted block, while the small prismatic body is hidden, and it is only weakly recognizable in the model obtained with the weighting function D.

D. Conductive Sources With Different Arrays

As a last synthetic test, we want to investigate whether different array types could affect the inversion of resistivity data. To this end, we considered four conductive bodies of 20 Ωm within a homogenous resistive background of 100 Ωm (see Fig. 11). The pseudosections of three geoelectric configurations are represented in Fig. 11: 1) a dipole–dipole array with

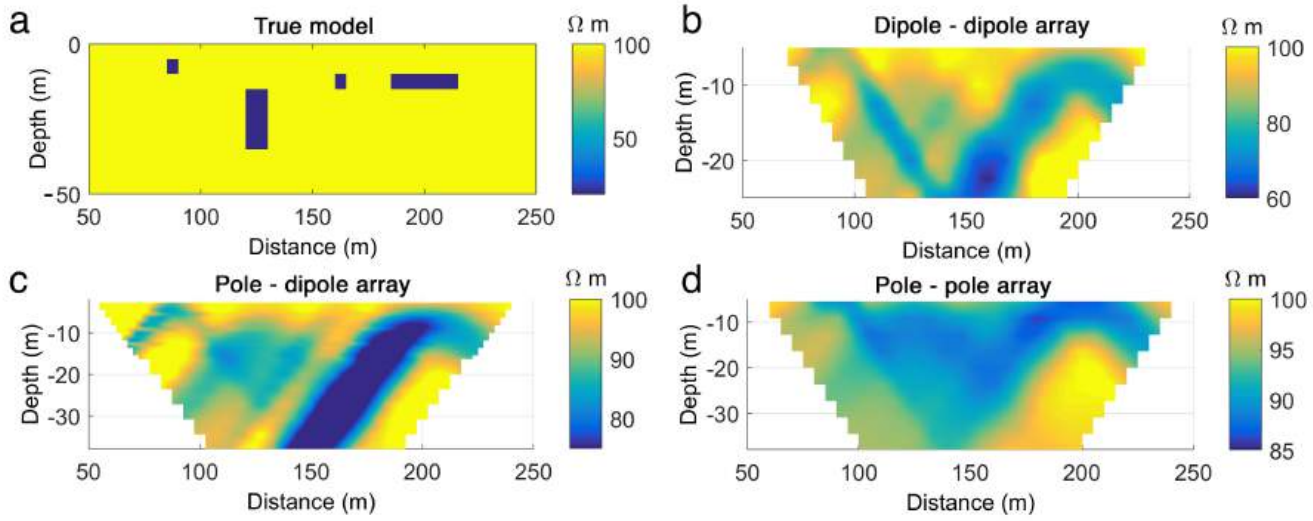

Fig. 11. (a) Resistivity model of four bodies (20 Ωm) in a homogeneous half-space (100 Ωm). (b) Apparent resistivity pseudosection for a dipole–dipole array. (c) Apparent resistivity pseudosection for a pole–dipole array. (d) Apparent resistivity pseudosection for and pole–pole arrays.

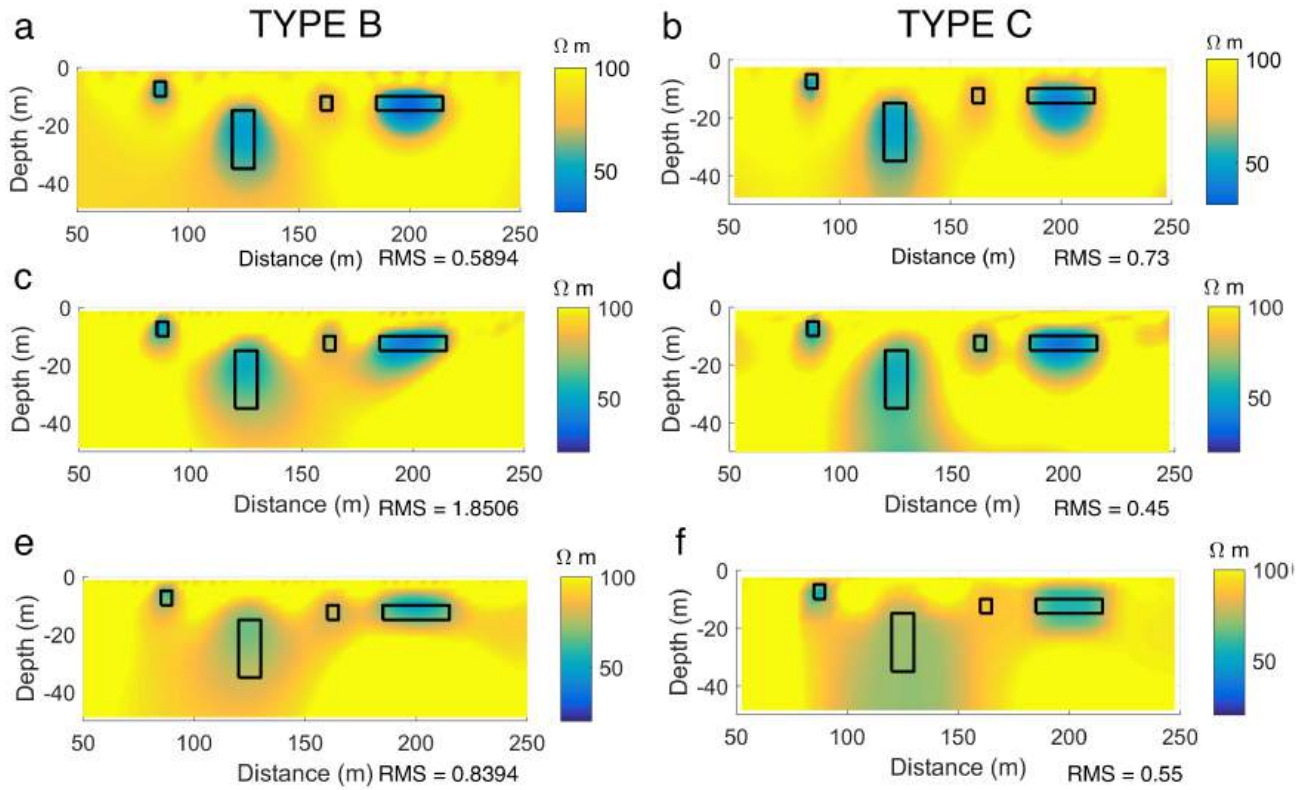

Fig. 12. Resistivity models from inversion of the data in Fig. 8 and for different arrays. (a) and (b) Using weighting functions of types B and C for a dipole–dipole array. (c) and (d) Weighting functions of types B and C for a pole–dipole array. (e) and (f) Weighting functions of types B and C for a pole–pole array. Solid boxes indicate the source outlines.

10-m dipole separation and n from 1 to 9; 2) a pole–dipole array with 5- (n from 1 to 8) and 10-m (n from 1 to 10) dipole separations; and 3) a pole–pole array with nine separations between current and potential electrodes from 5 to 45 m. For the sake of clarity, we used only model weighting of type B. Besides this, due to the results obtained in the previous sections, our choice for the exponent of the depth weighting was $\beta = 1$.

Resistivity models using weighting-model functions of types B and C are displayed in Fig. 12. In general, we find that both weighting functions yield good results for the shallowest sources, while the deepest source is not well reproduced

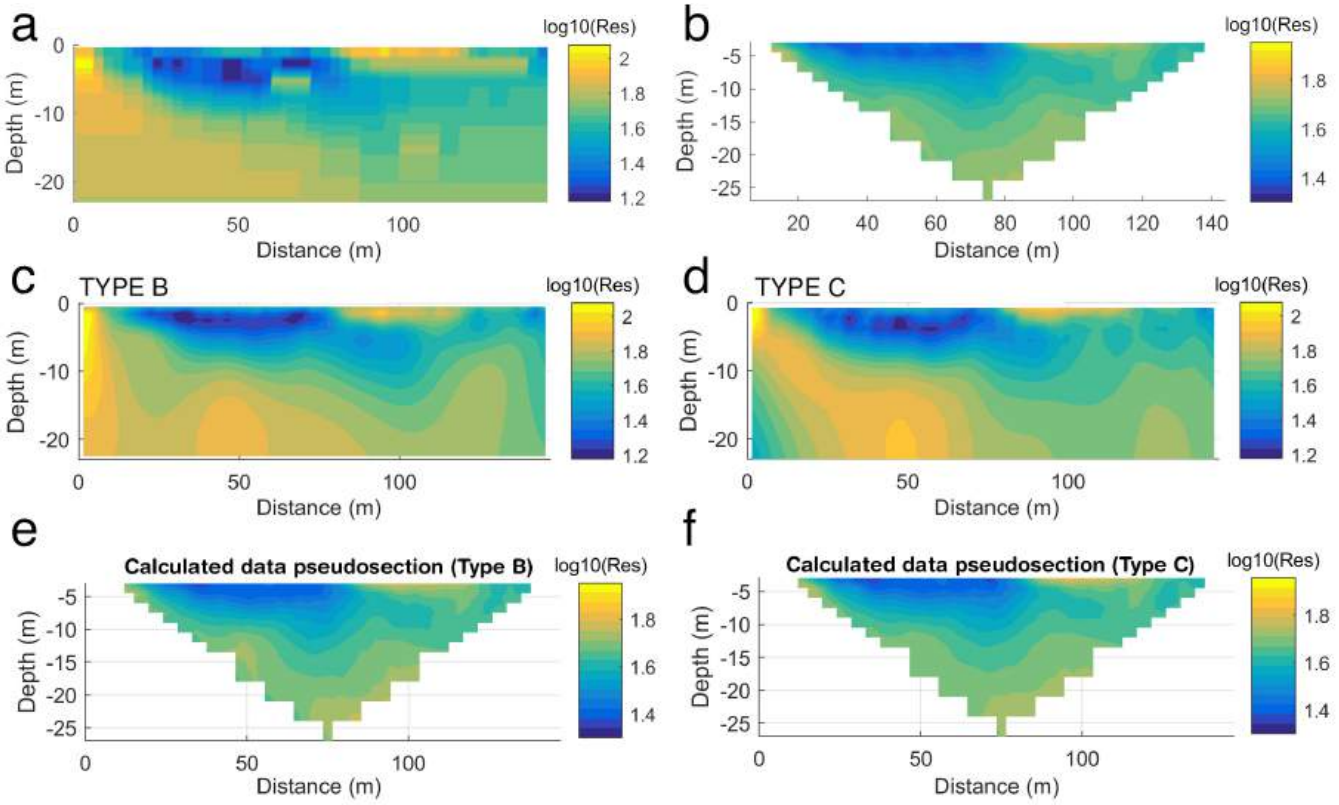

Fig. 13. (a) Criterion model of the landfill, as found from default models of RES2DMOD software (Büro für Geophysik Lorenz Company). (b) Resistivity data pseudosection. (c) Resistivity model using the weighting function of type B with $\beta = 1$. (d) Resistivity model using the weighting function of type C. (e) Pseudosection of computed data using the inverted model in (c). (f) Pseudosection of computed data using the inverted model in (d).

with the weighting function of type C. An interesting and quite unexpected result also occurs: the weighting function of type B gives consistent results no matter the array, while, with the weighting function of type C, the deep source is reconstructed better with the dipole–dipole array and poorly with the other arrays, yielding also too low values of resistivity. In conclusion, the weighting function of type B leads to better and more consistent results for all the considered arrays.

IV. Real Data

A. Landfill (Wenner Alpha Array)

Fig. 13(a) shows the criterion model of a waste deposit landfill in Berlin (Germany) and the relative pseudosection provided by the Büro für Geophysik Lorenz Company (http://www.geophysik-lorenz.de/pro.html). Data refer to the Wenner alpha array with electrode separations of 3 and 6 m [see Fig. 13(b)]. The subsurface is discretized into 49 and 25 cells in the x- and z-directions, all sized 3×1 m^2. Iterative inversion started with an initial homogeneous model of 50-Ωm resistivity. We show the models retrieved using weighting functions of type B with $\beta = 1$ and type C [see Fig. 13(c) and (d)]. We may observe that the model resistivities obtained using the weighting function of type B are closer to the resistivities of the criterion model shown in Fig. 13(a). At shallow depths, say from 0 to 10 m, the inferred models are similar, showing low resistivity values from 0 to 80 m along the x-axis and a very shallow resistive layer from $x = 80$ m to $x = 120$ m. We can instead observe substantial differences at greater depths, especially at the left corner, where the results obtained using the weighting function B are generally more similar to the original model. On the contrary, the resistivity model with the weighting function of type C has a lower resolution at depth and shows mostly low resistivity values. The regularization parameter and the number of iterations using the weighting function of type B are 0. 5 and 10, respectively. Fig. 13(e) and (f) shows the pseudosections computed from the models inverted with weighting functions of types C and B, respectively. The rms errors of data misfit for weighting function of types C and B models are 1.29% and 3.19%, respectively.

B. Mining (Dipole–Dipole Array)

Finally, we analyze the inversion of dc resistivity data in a mining district (Iran). This dataset was collected using a dipole–dipole array on Robat Sang mine, near Mashhad, Iran (see Fig. 14).

Segregation of the Afghan block from the bedrock throughout the time of the Cenomanian has brought about the displacement of the oceanic mantle and oceanic crust-associated ophiolitic bedrock in the area; this Ophiolite rock segment is situated at the basis of chromite and copper mineralization potential in the region [33]. The collision of the Arabian

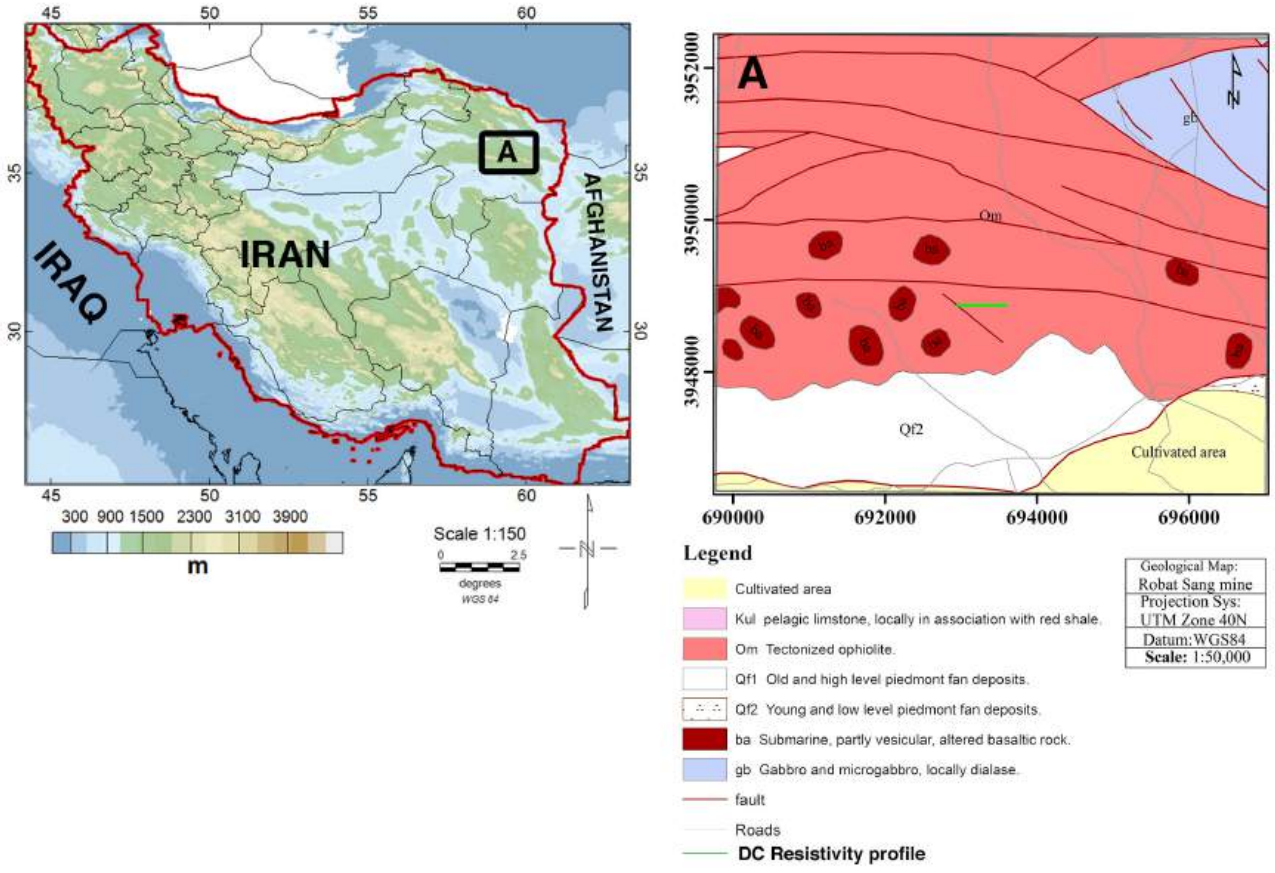

Fig. 14. (Left) Geographic map of Iran, the interested area is marked with a black rectangle. (Right) Geological map of the Robat Sang mine area, near Mashhad (courtesy of the Geological Survey of Iran).

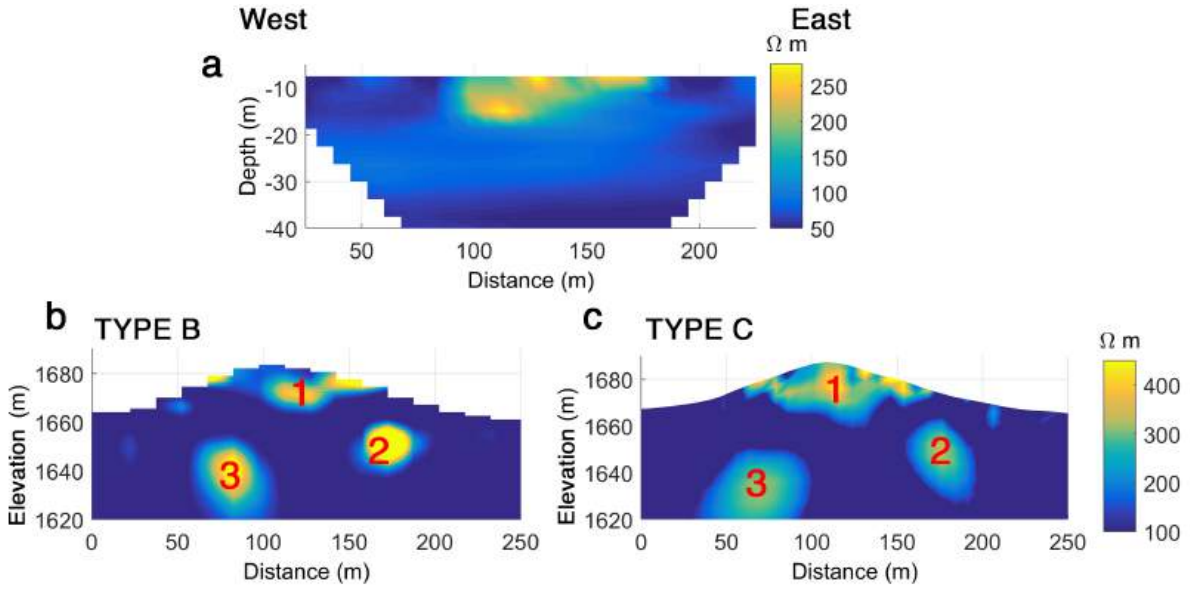

Fig. 15. Inversion of dc resistivity data in a mining district (Robat Sang, Iran). (a) Pseudosection of measured data along with the profile [green line in Fig. 14 (right)]. (b) LE resistivity model using the weighting function of type B with $\beta = 1$. (c) NLE resistivity model using a weighting function of type C.

Plateau on the Central Iranian Block gave rise to orogenic activities from north–northwest to south–southwest of most of Iran [33]. This structural pattern shows a very complicated structure and is denoting an intercontinental orogeny in these regions because of the right-handed rotations of the Lut and Hilmand Blocks [33]. This rotation is the principal reason for

the severe tectonics and the existence of disparate alteration zones in the area. Since this region includes active tectonics, the faults act as channels and engender the mineralization of copper carbonates (malachite) [34].

Dipole separation and the number of data were 15 m (with n from 1 to 10) and 128, respectively. The pseudosection of the measured data is represented in Fig. 15(a), and the reconstructed models derived from weighting functions of types B and C are displayed in Fig. 15(b) and (c), respectively. Both the inverted models show three resistive anomalies with a general agreement; however, we note some differences.

1) The two models of the shallowest source, close to the surface, are not coincident, and the NLE solution with the model weighting function of type C is noisier than the solution with the model weighting function of type B.

2) The deepest source for the model weighting function of type C has a lower resolution and tends to extend at depth, similar to the previous synthetic cases.

Finally, the sources with the weighting function of type B appear to be more resolved and have a higher resistivity contrast, which is in agreement with the expected resistivity of Malachite in alteration zones, ranging from 300 to 600 Ωm [35]. The rms errors of data misfit for weighting function of types C and B are 10.2% and 4.06%, respectively.

V. Conclusion

There are many inversion algorithms for the dc resistivity problem, either linear or nonlinear. However, the effects of the model weighting function on the source reconstruction have not been well discussed in the literature. For the gravity problem, such a kind of discussion is relatively more developed, especially related to the dependence on the weighting function of the average depth to the source (e.g., [3]).

As a matter of fact, the model weighting function inserts *a priori* information in the inverse problem, which is important for interpreting both gravity and dc resistivity data, and can be even more relevant for joint or cooperative inversion.

Thus, our intent was to compare the different behavior of gravity and resistivity inversions based on different types of model weighting: 1) depth weighting; 2) depth weighting and compactness; 3) roughness matrix for the L_2-norm nonlinear optimization method; and 4) roughness matrix for the L_1-norm nonlinear optimization method.

From the results obtained by synthetic and real data inversion, we may argue that both gravity and resistivity inversions are sensitive to the exponent β of depth weighting but in a different way. We, indeed, found that, for gravity, $\beta = 1$ works well for compact sources, while a much lower value, say $\beta = 0.1$, works for an interface model. To the best of our knowledge, this last result is important since it has not been discussed previously in the literature. In any case, compactness helps define with a high resolution both compact and interface source distributions so that a weighting function of type B is the most suitable choice.

Instead, for resistivity data inversion, we found an optimal value $\beta = 1$, working well for both compact and interface models, as well as more complex source distributions. In general, we reached good solutions also with other values of the depth weighting exponent, but, with values other than $\beta = 1$, the number of iterations increases dramatically.

For the resistivity data inversion, we also found that the roughness matrix (weighting function of types C and D) tends to yield a poorer resolution at large depth, despite using the L_1- or L_2-norm*s*.

Finally, we found that the response from different arrays is appreciably coherent with the weighting function based on the depth weighting/compactness (weighting functions of types A and B), while the roughness matrix (weighting functions of types C and D) seems less able to reproduce consistent source models.

References

[1] M. A. Pérez-Flores, S. Méndez-Delgado, and E. Gómez-Treviño, "Imaging low-frequency and DC electromagnetic fields using a simple linear approximation," *Geophysics*, vol. 66, no. 4, pp. 1067–1081, Jul. 2001.

[2] Y. Li and D. W. Oldenburg, "3-D inversion of gravity data," *Geophysics*, vol. 63, no. 1, pp. 109–119, Jan. 1998.

[3] F. Cella and M. Fedi, "Inversion of potential field data using the structural index as weighting function rate decay," *Geophys. Prospecting*, vol. 60, no. 2, pp. 313–336, Mar. 2012.

[4] N. C. Smith and K. Vozoff, "Two-dimensional DC resistivity inversion for dipole-dipole data," *IEEE Trans. Geosci. Remote Sens.*, vol. GE-22, no. 1, pp. 21–28, Jan. 1984.

[5] Y. Sasaki, "3-D resistivity inversion using the finite-element method," *Geophysics*, vol. 59, no. 12, pp. 1839–1848, 1994.

[6] M. H. Loke and T. Dahlin, "A combined Gauss–Newton and quasi-Newton inversion method for the interpretation of apparent resistivity pseudosections," in *Proc. 3rd EEGS Meeting*, 1997, pp. 1–4.

[7] M. H. Loke and T. Dahlin, "A comparison of the Gauss–Newton and quasi-Newton methods in resistivity imaging inversion," *J. Appl. Geophys.*, vol. 49, no. 3, pp. 149–162, Mar. 2002.

[8] E. Auken and A. V. Christiansen, "Layered and laterally constrained 2D inversion of resistivity data," *Geophysics*, vol. 69, no. 3, pp. 752–761, May 2004.

[9] T. Günther, C. Rücker, and K. Spitzer, "Three-dimensional modelling and inversion of DC resistivity data incorporating topography—II. Inversion," *Geophys. J. Int.*, vol. 166, no. 2, pp. 506–517, Aug. 2006.

[10] S. Boonchaisuk, C. Vachiratienchai, and W. Siripunvaraporn, "Two-dimensional direct current (DC) resistivity inversion: Data space Occam's approach," *Phys. Earth Planet. Interiors*, vol. 168, nos. 3–4, pp. 204–211, Jul. 2008.

[11] N. G. Papadopoulos, P. Tsourlos, C. Papazachos, G. N. Tsokas, A. Sarris, and J. H. Kim, "An algorithm for fast 3D inversion of surface electrical resistivity tomography data: Application on imaging buried antiquities," *Geophys. Prospecting*, vol. 59, no. 3, pp. 557–575, May 2011.

[12] I. Demirci, E. Erdoğan, and M. E. Candansayar, "Two-dimensional inversion of direct current resistivity data incorporating topography by using finite difference techniques with triangle cells: Investigation of Kera fault zone in western Crete," *Geophysics*, vol. 77, no. 1, pp. E67–E75, Jan. 2012.

[13] T. Wiese, S. Greenhalgh, B. Zhou, M. Greenhalgh, and L. Marescot, "Resistivity inversion in 2-D anisotropic media: Numerical experiments," *Geophys. J. Int.*, vol. 201, no. 1, pp. 247–266, Apr. 2015.

[14] T.-K. Chou, M. Chouteau, and J.-S. Dubé, "Intelligent meshing technique for 2D resistivity inverse problems," *Geophysics*, vol. 81, no. 4, pp. IM45–IM56, Jul. 2016.

[15] N. Y. Gündoğdu and M. E. Candansayar, "Three-dimensional regularized inversion of DC resistivity data with different stabilizing functionals," *Geophysics*, vol. 83, no. 6, pp. E399–E407, Nov. 2018.

[16] B. Last and K. Kubik, "Compact gravity inversion," *Geophysics*, vol. 48, no. 6, pp. 713–721, 1983.

[17] O. Portniaguine and M. S. Zhdanov, "Focusing geophysical inversion images," *Geophysics*, vol. 64, no. 3, pp. 874–887, May 1999.

[18] O. Boulanger and M. Chouteau, "Constraints in 3D gravity inversion," *Geophys. Prospecting*, vol. 49, no. 2, pp. 265–280, Dec. 2001.

[19] V. Paoletti, S. Ialongo, G. Florio, M. Fedi, and F. Cella, "Self-constrained inversion of potential fields," *Geophys. J. Int.*, vol. 195, no. 2, pp. 854–869, Nov. 2013.

[20] A. Vitale and M. Fedi, "Self-constrained inversion of potential fields through a 3D depth weighting," *Geophysics*, vol. 85, no. 6, pp. G143–G156, Nov. 2020.
[21] M. Milano, R. Varfinezhad, H. Bizhani, M. Moghadasi, A. N. Kalateh, and H. Baghzendani, "Joint interpretation of magnetic and gravity data at the Golgohar mine in Iran," *J. Appl. Geophys.*, vol. 195, Dec. 2021, Art. no. 104476.
[22] W. Menke, *Geophysical Data Analysis: Discrete Inverse Theory*. New York, NY, USA: Academic, 2012.
[23] R. Varfinezhad, B. Oskooi, and M. Fedi, "Joint inversion of DC resistivity and magnetic data, constrained by cross gradients, compactness and depth weighting," *Pure Appl. Geophys.*, vol. 177, no. 9, pp. 4325–4343, Sep. 2020.
[24] M. H. Loke, I. Acworth, and T. Dahlin, "A comparison of smooth and blocky inversion methods in 2D electrical imaging surveys," *Explor. Geophys.*, vol. 34, no. 3, pp. 182–187, Jun. 2003.
[25] Y. Li and D. W. Oldenburg, "Approximate inverse mappings in DC resistivity problems," *Geophys. J. Int.*, vol. 109, no. 2, pp. 343–362, May 1992.
[26] A. S. Charré-Meza, M. A. Pérez-Flores, and E. Gómez-Treviño, "2-D inversion of DC resistivity data from the cerro prieto geothermal area, Mexico," in *Proc. World Geothermal Congr.*, Jun. 2000, pp. 1–5.
[27] M. H. Loke, "Rapid 2D resistivity forward modeling using the finite difference and finite element methods," RES2DMOD ver 3, 2002, pp. 1996–2002.
[28] Y. Li and D. W. Oldenburg, "Fast inversion of large-scale magnetic data using wavelet transforms and a logarithmic barrier method," *Geophys. J. Int.*, vol. 152, no. 2, pp. 251–265, Feb. 2003.
[29] R. Wolke and H. Schwetlick, "Iteratively reweighted least squares: Algorithms, convergence analysis, and numerical comparisons," *SIAM J. Sci. Stat. Comput.*, vol. 9, no. 5, pp. 907–921, 1988.
[30] M. S. Zhdanov, *Geophysical Inverse Theory and Regularization Problems*. Amsterdam, The Netherlands: Elsevier, 2002.
[31] S. Vitale *et al.*, "Seismically induced soft-sediment deformation phenomena during the volcano-tectonic activity of Campi Flegrei caldera (southern Italy) in the last 15 kyr," *Tectonics*, vol. 38, no. 6, pp. 1999–2018, 2019.
[32] M. H. Loke. (2004). *2-D and 3-D Electrical Imaging Surveys*. [Online]. Available: http://www.geoelectrical.com
[33] M. Berberian and G. C. P. King, "Towards a paleogeography and tectonic evolution of Iran," *Can. J. Earth Sci.*, vol. 18, no. 2, pp. 210–265, Feb. 1981.
[34] G. Mahdavi, A. Khakzad, and M. Lotfi, "Conditions of ore-mineralization and geochemical correlation of rare-elements at the Robat Pb-Zn deposit, west of Khomein, central Iran," *Open J. Geol.*, vol. 6, no. 9, pp. 1118–1136, 2016.
[35] M. Bemani, S. H. Mojtahedzadeh, and A. Ansari, "Investigation and adaptation of geophysical data with alteration zones of Aliabad Damak copper deposit," *J. Mineral Resour. Eng.*, vol. 4, no. 1, pp. 21–43, 2019.

Ramin Varfinezhad was born in Kermanshah, Iran, in 1988. He received the B.S. degree in solid-state physics from the University of Urmia, Urmia, Iran, in 2011, and the M.S. and Ph.D. degrees in geophysics from the University of Tehran, Tehran, Iran, in 2014 and 2020, respectively.

His research interests include forward modeling and inversion of magnetic, gravity, dc resistivity and frequency domain electromagnetic (FDEM) methods, and geophysical data integration as joint inversion and joint interpretation.

Maurizio Fedi received the M.Sc. degree in physics and the Ph.D. degree in applied geophysics from the University of Naples Federico II, Naples, Italy, in 1982 and 1987, respectively.

He was a Researcher with the University of Naples Federico II from 1990 to 1992 and an Associate Professor with the University of Lecce, Lecce, Italy, from 1992 to 1996, and the University of Naples Federico II from 1996 to 2000. He was a Visiting Professor with The University of British Columbia, Vancouver, BC, Canada, the China University of Geosciences, Beijing, China, the National Geophysical Research Institute (NGRI), Hyderabad, India, the University of Tehran, Tehran, Iran, and the China University of Geosciences, Wuhan, China. He has been a Full Professor with the Department of Earth, Environmental and Resource Science, University of Naples Federico II, since 2000. He is the author of more than 250 articles in international scientific journals and books. His research interests include potential field inversion and imaging, multifractal analysis, developments of interpretation techniques for DC resistivity, ground penetrating radar (GPR), frequency domain electromagnetic (FDEM), and controlled source electromagnetic (CSEM) methods, integrated fields, and modeling geophysics.

Dr. Fedi was an Invited Speaker at international conferences, such as South African Geophysical Association (SAGA), Asia Oceania Geosciences Society (AOGS), Italian Society of Industrial and Applied Mathematics (SIMAI), GM Hangzhou, the Morlet's-Wavelet-Symposium, European Geosciences Union (EGU), and 2018 EAGE, Oporto. He is also the Co-Editor-in-Chief of the *Journal of Applied Geophysics* (Elsevier).

Maurizio Milano received the M.S. degree in geophysics and applied geophysics and the Ph.D. degree in Earth, environment, and resources sciences from the University of Naples Federico II, Naples, Italy, in 2009 and 2017, respectively.

He was a Post-Doctoral Research Fellow with the L.U.P.T. Interdepartmental Center, University of Naples Federico II, from 2017 to 2019, and the Institute of Marine Sciences of Naples—National Research Council (ISMAR-CNR), Naples, from 2019 to 2021. He is currently a Researcher in applied geophysics with the Department of Earth, Environment and Resources Sciences, University of Naples Federico II. His research interests include multiscale potential fields' analysis for modeling the lower crust; potential field satellite data modeling for the interpretation of the Earth's core dynamics; and inversion of gravity field data for modeling of geothermal reservoirs.